BNL-219906-2020-JAAM

Measurement of Groomed Jet Substructure Observables in p+p Collisions at ps = 200 GeV with STAR

J. Adam

To be published in "Physics Letters B"

October 2020

Physics Department

Brookhaven National Laboratory

U.S. Department of Energy

USDOE Office of Science (SC), Nuclear Physics (NP) (SC-26)

Notice: This manuscript has been authored by employees of Brookhaven Science Associates, LLC under Contract No. DE-SC0012704 with the U.S. Department of Energy. The publisher by accepting the manuscript for publication acknowledges that the United States Government retains a non-exclusive, paid-up, irrevocable, world-wide license to publish or reproduce the published form of this manuscript, or allow others to do so, for United States Government purposes.

DISCLAIMER

This report was prepared as an account of work sponsored by an agency of the United States Government. Neither the United States Government nor any agency thereof, nor any of their employees, nor any of their contractors, subcontractors, or their employees, makes any warranty, express or implied, or assumes any legal liability or responsibility for the accuracy, completeness, or any third party's use or the results of such use of any information, apparatus, product, or process disclosed, or represents that its use would not infringe privately owned rights. Reference herein to any specific commercial product, process, or service by trade name, trademark, manufacturer, or otherwise, does not necessarily constitute or imply its endorsement, recommendation, or favoring by the United States Government or any agency thereof or its contractors or subcontractors. The views and opinions of authors expressed herein do not necessarily state or reflect those of the United States Government or any agency thereof.

arXiv:2003.02114v1 [hep-ex] 4 Mar 2020

Measurement of Groomed Jet Substructure Observables in p+p Collisions at $\sqrt{s}$ = 200 GeV with STAR

J. Adam[6], L. Adamczyk[2], J. R. Adams[39], J. K. Adkins[30], G. Agakishiev[28], M. M. Aggarwal[40], Z. Ahammed[59], I. Alekseev[3,35], D. M. Anderson[53], A. Aparin[28], E. C. Aschenauer[6], M. U. Ashraf[11], F. G. Atetalla[29], A. Attri[40], G. S. Averichev[28], V. Bairathi[22], K. Barish[10], A. Behera[51], R. Bellwied[20], A. Bhasin[27], J. Bielcik[14], J. Bielcikova[38], L. C. Bland[6], I. G. Bordyuzhin[3], J. D. Brandenburg[48,6], A. V. Brandin[35], J. Butterworth[44], H. Caines[62], M. Calderón de la Barca Sánchez[8], D. Cebra[8], I. Chakaberia[29,6], P. Chaloupka[14], B. K. Chan[9], F-H. Chang[37], Z. Chang[6], N. Chankova-Bunzarova[28], A. Chatterjee[11], D. Chen[10], J. H. Chen[18], X. Chen[47], Z. Chen[48], J. Cheng[55], M. Cherney[13], M. Chevalier[10], S. Choudhury[18], W. Christie[6], H. J. Crawford[7], M. Csanád[16], M. Daugherity[1], T. G. Dedovich[28], I. M. Deppner[19], A. A. Derevschikov[42], L. Didenko[6], X. Dong[31], J. L. Drachenberg[1], J. C. Dunlop[6], T. Edmonds[43], N. Elsey[61], J. Engelage[7], G. Eppley[44], R. Esha[51], S. Esumi[56], O. Evdokimov[12], A. Ewigleben[32], O. Eyser[6], R. Fatemi[30], S. Fazio[6], P. Federic[38], J. Fedorisin[28], C. J. Feng[37], Y. Feng[43], P. Filip[28], E. Finch[50], Y. Fisyak[6], A. Francisco[62], L. Fulek[2], C. A. Gagliardi[53], T. Galatyuk[15], F. Geurts[44], A. Gibson[58], K. Gopal[23], D. Grosnick[58], W. Guryn[6], A. I. Hamad[29], A. Hamed[5], J. W. Harris[62], S. He[11], W. He[18], X. He[26], S. Heppelmann[8], S. Heppelmann[41], N. Herrmann[19], E. Hoffman[20], L. Holub[14], Y. Hong[31], S. Horvat[62], Y. Hu[18], H. Z. Huang[9], S. L. Huang[51], T. Huang[37], X. Huang[55], T. J. Humanic[39], P. Huo[51], G. Igo[9], D. Isenhower[1], W. W. Jacobs[25], C. Jena[23], A. Jentsch[6], Y. JI[47], J. Jia[6,51], K. Jiang[47], S. Jowzaee[61], X. Ju[47], E. G. Judd[7], S. Kabana[29], M. L. Kabir[10], S. Kagamaster[32], D. Kalinkin[25], K. Kang[55], D. Kapukchyan[10], K. Kauder[6], H. W. Ke[6], D. Keane[29], A. Kechechyan[28], M. Kelsey[31], Y. V. Khyzhniak[35], D. P. Kikoła [60], C. Kim[10], B. Kimelman[8], D. Kincses[16], T. A. Kinghorn[8], I. Kisel[17], A. Kiselev[6], A. Kisiel[60], M. Kocan[14], L. Kochenda[35], L. K. Kosarzewski[14], L. Kramarik[14], P. Kravtsov[35], K. Krueger[4], N. Kulathunga Mudiyanselage[20], L. Kumar[40], R. Kunnawalkam Elayavalli[61], J. H. Kwasizur[25], R. Lacey[51], S. Lan[11], J. M. Landgraf[6], J. Lauret[6], A. Lebedev[6], R. Lednicky[28], J. H. Lee[6], Y. H. Leung[31], C. Li[47], W. Li[44], W. Li[49], X. Li[47], Y. Li[55], Y. Liang[29], R. Licenik[38], T. Lin[53], Y. Lin[11], M. A. Lisa[39], F. Liu[11], H. Liu[25], P. Liu[51], P. Liu[49], T. Liu[62], X. Liu[39], Y. Liu[53], Z. Liu[47], T. Ljubicic[6], W. J. Llope[61], R. S. Longacre[6], N. S. Lukow[52], S. Luo[12], X. Luo[11], G. L. Ma[49], L. Ma[18], R. Ma[6], Y. G. Ma[49], N. Magdy[12], R. Majka[62], D. Mallick[36], S. Margetis[29], C. Markert[54], H. S. Matis[31], J. A. Mazer[45], N. G. Minaev[42], S. Mioduszewski[53], B. Mohanty[36], M. M. Mondal[51], I. Mooney[61], Z. Moravcova[14], D. A. Morozov[42], M. Nagy[16], J. D. Nam[52], Md. Nasim[22], K. Nayak[11], D. Neff[9], J. M. Nelson[7], D. B. Nemes[62], M. Nie[48], G. Nigmatkulov[35], T. Niida[56], L. V. Nogach[42], T. Nonaka[11], G. Odyniec[31], A. Ogawa[6], S. Oh[31], V. A. Okorokov[35], B. S. Page[6], R. Pak[6], A. Pandav[36], Y. Panebratsev[28], B. Pawlik[2], D. Pawlowska[60], H. Pei[11], C. Perkins[7], L. Pinsky[20], R. L. Pintér[16], J. Pluta[60], J. Porter[31], M. Posik[52], N. K. Pruthi[40], M. Przybycien[2], J. Putschke[61], H. Qiu[26], A. Quintero[52], S. K. Radhakrishnan[29], S. Ramachandran[30], R. L. Ray[54], R. Reed[32], H. G. Ritter[31], J. B. Roberts[44], O. V. Rogachevskiy[28], J. L. Romero[8], L. Ruan[6],

J. Rusnak[38], N. R. Sahoo[48], H. Sako[56], S. Salur[45], J. Sandweiss[62], S. Sato[56], W. B. Schmidke[6], N. Schmitz[33], B. R. Schweid[51], F. Seck[15], J. Seger[13], M. Sergeeva[9], R. Seto[10], P. Seyboth[33], N. Shah[24], E. Shahaliev[28], P. V. Shanmuganathan[6], M. Shao[47], F. Shen[48], W. Q. Shen[49], S. S. Shi[11], Q. Y. Shou[49], E. P. Sichtermann[31], R. Sikora[2], M. Simko[38], J. Singh[40], S. Singha[26], N. Smirnov[62], W. Solyst[25], P. Sorensen[6], H. M. Spinka[4], B. Srivastava[43], T. D. S. Stanislaus[58], M. Stefaniak[60], D. J. Stewart[62], M. Strikhanov[35], B. Stringfellow[43], A. A. P. Suaide[46], M. Sumbera[38], B. Summa[41], X. M. Sun[11], Y. Sun[47], Y. Sun[21], B. Surrow[52], D. N. Svirida[3], P. Szymanski[60], A. H. Tang[6], Z. Tang[47], A. Taranenko[35], T. Tarnowsky[34], J. H. Thomas[31], A. R. Timmins[20], D. Tlusty[13], M. Tokarev[28], C. A. Tomkiel[32], S. Trentalange[9], R. E. Tribble[53], P. Tribedy[6], S. K. Tripathy[16], O. D. Tsai[9], Z. Tu[6], T. Ullrich[6], D. G. Underwood[4], I. Upsal[48,6], G. Van Buren[6], J. Vanek[38], A. N. Vasiliev[42], I. Vassiliev[17], F. Videbæk[6], S. Vokal[28], S. A. Voloshin[61], F. Wang[43], G. Wang[9], J. S. Wang[21], P. Wang[47], Y. Wang[11], Y. Wang[55], Z. Wang[48], J. C. Webb[6], P. C. Weidenkaff[19], L. Wen[9], G. D. Westfall[34], H. Wieman[31], S. W. Wissink[25], R. Witt[57], Y. Wu[10], Z. G. Xiao[55], G. Xie[31], W. Xie[43], H. Xu[21], N. Xu[31], Q. H. Xu[48], Y. F. Xu[49], Y. Xu[48], Z. Xu[6], Z. Xu[9], C. Yang[48], Q. Yang[48], S. Yang[6], Y. Yang[37], Z. Yang[11], Z. Ye[44], Z. Ye[12], L. Yi[48], K. Yip[6], H. Zbroszczyk[60], W. Zha[47], D. Zhang[11], S. Zhang[47], S. Zhang[49], X. P. Zhang[55], Y. Zhang[47], Y. Zhang[11], Z. J. Zhang[37], Z. Zhang[6], J. Zhao[43], C. Zhong[49], C. Zhou[49], X. Zhu[55], Z. Zhu[48], M. Zurek[31], M. Zyzak[17]

[1]*Abilene Christian University, Abilene, Texas 79699*

[2]*AGH University of Science and Technology, FPACS, Cracow 30-059, Poland*

[3]*Alikhanov Institute for Theoretical and Experimental Physics NRC "Kurchatov Institute", Moscow 117218, Russia*

[4]*Argonne National Laboratory, Argonne, Illinois 60439*

[5]*American University of Cairo, New Cairo 11835, New Cairo, Egypt*

[6]*Brookhaven National Laboratory, Upton, New York 11973*

[7]*University of California, Berkeley, California 94720*

[8]*University of California, Davis, California 95616*

[9]*University of California, Los Angeles, California 90095*

[10]*University of California, Riverside, California 92521*

[11]*Central China Normal University, Wuhan, Hubei 430079*

[12]*University of Illinois at Chicago, Chicago, Illinois 60607*

[13]*Creighton University, Omaha, Nebraska 68178*

[14]*Czech Technical University in Prague, FNSPE, Prague 115 19, Czech Republic*

[15]*Technische Universität Darmstadt, Darmstadt 64289, Germany*

[16]*ELTE Eötvös Loránd University, Budapest, Hungary H-1117*

[17]*Frankfurt Institute for Advanced Studies FIAS, Frankfurt 60438, Germany*

[18]*Fudan University, Shanghai, 200433*

[19]*University of Heidelberg, Heidelberg 69120, Germany*

[20]*University of Houston, Houston, Texas 77204*

[21]*Huzhou University, Huzhou, Zhejiang 313000*

[22]*Indian Institute of Science Education and Research (IISER), Berhampur 760010 , India*

[23]*Indian Institute of Science Education and Research (IISER) Tirupati, Tirupati 517507, India*

[24]*Indian Institute Technology, Patna, Bihar 801106, India*

[25]*Indiana University, Bloomington, Indiana 47408*

[26]*Institute of Modern Physics, Chinese Academy of Sciences, Lanzhou, Gansu 730000*

[27]*University of Jammu, Jammu 180001, India*

[28]*Joint Institute for Nuclear Research, Dubna 141 980, Russia*

[29]*Kent State University, Kent, Ohio 44242*

[30]*University of Kentucky, Lexington, Kentucky 40506-0055*

[31]*Lawrence Berkeley National Laboratory, Berkeley, California 94720*

[32]*Lehigh University, Bethlehem, Pennsylvania 18015*

[33]*Max-Planck-Institut für Physik, Munich 80805, Germany*

[34]*Michigan State University, East Lansing, Michigan 48824*

[35]*National Research Nuclear University MEPhI, Moscow 115409, Russia*

[36]*National Institute of Science Education and Research, HBNI, Jatni 752050, India*

[37]*National Cheng Kung University, Tainan 70101*

[38]*Nuclear Physics Institute of the CAS, Rez 250 68, Czech Republic*

[39]*Ohio State University, Columbus, Ohio 43210*

[40]*Panjab University, Chandigarh 160014, India*

[41]*Pennsylvania State University, University Park, Pennsylvania 16802*

[42]*NRC "Kurchatov Institute", Institute of High Energy Physics, Protvino 142281, Russia*

[43]*Purdue University, West Lafayette, Indiana 47907*

[44]*Rice University, Houston, Texas 77251*

[45]*Rutgers University, Piscataway, New Jersey 08854*

[46]*Universidade de São Paulo, São Paulo, Brazil 05314-970*

[47]*University of Science and Technology of China, Hefei, Anhui 230026*

[48]*Shandong University, Qingdao, Shandong 266237*

[49]*Shanghai Institute of Applied Physics, Chinese Academy of Sciences, Shanghai 201800*

[50]*Southern Connecticut State University, New Haven, Connecticut 06515*

[51]*State University of New York, Stony Brook, New York 11794*

[52]*Temple University, Philadelphia, Pennsylvania 19122*

[53]*Texas A&M University, College Station, Texas 77843*

[54] University of Texas, Austin, Texas 78712
[55] Tsinghua University, Beijing 100084
[56] University of Tsukuba, Tsukuba, Ibaraki 305-8571, Japan
[57] United States Naval Academy, Annapolis, Maryland 21402
[58] Valparaiso University, Valparaiso, Indiana 46383
[59] Variable Energy Cyclotron Centre, Kolkata 700064, India
[60] Warsaw University of Technology, Warsaw 00-661, Poland
[61] Wayne State University, Detroit, Michigan 48201
[62] Yale University, New Haven, Connecticut 06520

Abstract

In this letter, a comprehensive suite of jet substructure measurements via the Soft-Drop algorithm, including the shared momentum fraction (z_{g}) and the groomed jet radius (R_{g}), are reported in p+p collisions at $\sqrt{s}$ = 200 GeV collected by the STAR experiment. These substructure observables are differentially measured for jets of varying resolution parameters from $R = 0.2$ to $R = 0.6$ and transverse momentum range $15 < p_{\mathrm{T,jet}} < 60$ GeV/c. These studies show that, at RHIC kinematics with increasing jet resolution parameter and jet energy, the z_{g} distribution asymptotically converges to the DGLAP splitting kernel. The groomed jet radius measurements reflect a momentum-dependent narrowing of the jet structure for jets of a given resolution parameter, i.e., the larger the $p_{\mathrm{T,jet}}$, the narrower the first split. For the first time, these fully corrected measurements are compared to leading order Monte Carlo generators and to state-of-the-art theoretical calculations at next-to-leading-log accuracy. We observe that RHIC-tuned PYTHIA 6 is able to quantitatively reproduce data whereas the LHC-tuned event generators, PYTHIA 8 and HERWIG 7, are unable to provide a simultaneous description of both the z_{g} and R_{g}, resulting in opportunities for fine parameter tuning of these models in p+p collisions at varying collision energies. We also find that the theoretical calculations without non-perturbative corrections are able to qualitatively describe the trend in data for jets of large resolution parameters at high $p_{\mathrm{T,jet}}$, but fail at small jet resolution parameters and low jet momenta.

Keywords: jet substructure, SoftDrop, splitting function, groomed jet radius

1. Introduction

Jets are well-established signals of partons, i.e., quarks and gluons, created in the hard scatterings during high energy hadron collisions [1]. Jets have played a prominent role as an internal probe of partonic energy loss mechanisms in the quark-gluon plasma created in heavy-ion collisions. Refer to [2] and [3] for recent reviews of the experimental measurements and theoretical calculations on jet quenching. An important prerequisite of such studies is a quantitative understanding of jet properties related to its production, evolution and hadronization. The production of hard scattered partons is governed by $2 \rightarrow 2$ quantum chromodynamics (QCD) scattering at leading order (LO) and $2 \rightarrow 3$ at next-to-leading order (NLO), and is calculable using Parton Distribution Functions (PDFs) [4], which are extracted with fits to experimental measurements, including but not limited to jet cross-sections at various kinematics. Given a hard scattered parton, the Dokshitzer-Gribov-Lipatov-Altarelli-Parisi (DGLAP) splitting kernels [5, 6, 7] describe its evolution and fragmentation based on perturbative quantum chromodynamics (pQCD). At LO, the DGLAP splitting functions of a parton in vacuum are dependent on the momentum fraction of the radiated gluon and the corresponding angle of emission. The most efficient way for a highly virtual/off-shell parton to lose its virtuality is via consecutive radiation/splitting (for example $q \rightarrow q+g$), resulting in a parton shower. Due to the double logarithmic structure of the splitting kernels and color coherence in the QCD, the evolution is expected to follow an angular or virtuality ordered shower. Such an ordering implies that the earliest splits are soft and wide in angle with the harder (referring to a high momentum radiated gluon) collinear splits happening later during jet evolution. Therefore, this process can be described by two natural scales: the split's momentum fraction and its angle with respect to the parton direction which, in turn, describe jet structure in vacuum. The primary focus of this letter is to study QCD and parton evolution in p+p collisions at RHIC. We establish a quantitative description of jet substructure that can serve as a reference for comparison to similar measurements in heavy-ion collisions where jet properties are

expected to be modified due to jet quenching effects.

In this letter, we present fully corrected measurements of the SoftDrop groomed momentum fraction ($z_{\rm g}$) and the groomed jet radius ($R_{\rm g}$) in p+p collisions at center-of-mass energy $\sqrt{s}$ = 200 GeV. They allow a direct measurement of the DGLAP splitting functions during jet evolution. These measurements emerge as a "by-product" of the modified mass drop tagger or SoftDrop [8, 9, 10] grooming algorithm, used to remove soft, wide-angle radiation from sequentially clustered jets. This is achieved by recursively de-clustering the jet's angular-ordered branching history via the Cambridge/Aachen (C/A) clustering algorithm [11, 12], which sequentially combines nearest constituents, i.e., those located closest in angle. Subjets are discarded until the transverse momenta, $p_{\rm T,1}$ and $p_{\rm T,2}$, of the subjets from the current splitting fulfill the SoftDrop condition, $z_{\rm g} = \frac{\min(p_{\rm T,1}, p_{\rm T,2})}{p_{\rm T,1}+p_{\rm T,2}} > z_{\rm cut}\left(\frac{R_{\rm g}}{R}\right)^{\beta}$, where $R_{\rm g}$ is the groomed jet radius or a measure of the distance as defined in pseudorapidity-azimuthal angle ($\eta - \phi$) space between the two surviving subjets and R is the jet resolution parameter. This analysis sets $\beta = 0$ and a momentum fraction cut of $z_{\rm cut} = 0.1$ [9] to determine if a subjet at a given clustering step survives the grooming procedure. The $z_{\rm cut}$ parameter is set to reduce sensitivity to non-perturbative effects arising from the underlying event and hadronization [9, 13]. It has been shown that for such a choice of $z_{\rm cut}$ and β, along with the usage of the C/A algorithm for de-clustering, the distribution of the resulting $z_{\rm g}$ converges to the vacuum DGLAP splitting functions for $z > z_{\rm cut}$ in a "Sudakov-safe" manner [10], i.e., independent of the strong coupling constant (α_s) in the ultraviolet (UV) limit and under the fixed coupling approximation. Since the splitting kernels are defined to be independent of the momenta of initial partons, the UV limit corresponds to a jet of infinite momentum.

The SoftDrop $z_{\rm g}$ was first measured by the CMS collaboration in p+p and Pb+Pb collisions at $\sqrt{s_{\rm NN}}$ = 5.02 TeV at the LHC for highly energetic jets with $p_{\rm T,jet} > 140$ GeV/c [14]. As the measurements are not corrected for smearing due to detector effects and resolution in Pb+Pb, the Monte Carlo (MC) generators, such as PYTHIA 6 [15], PYTHIA 8 [16] and HERWIG++ [17, 18], are smeared instead to make meaningful comparisons. Due to the granularity of the CMS calorimeter, a $R_{\rm g} > 0.1$ threshold was enforced which consequently introduced a bias towards wider jets in the study [19]. It

was shown that event generators at the LHC generally reproduce the trend in p+p collisions, but individually, neither PYTHIA 8 nor HERWIG 7 were able to quantitatively describe the measurements within systematic uncertainties. The large center-of-mass energies at the LHC increases NLO effects in jet production and fragmentation along with an increased sensitivity to multi-parton interactions and pileup. On the other hand, due to their large jet p_{T}, the measurements are less sensitive to the hadronization process and higher-order power corrections [20, 21] due to a small α_{s}.

The p+p collisions at RHIC provide a complementary environment to study the jet structure and parton evolution. Due to the reduced center-of-mass energy (200 GeV as compared to 5.02 TeV), the study offers further insights regarding jet evolution by exploring different contributions of NLO effects and hadronization. For example, the higher-order effects in jet production at RHIC are suppressed compared to the LHC, while jets at RHIC are more susceptible to non-perturbative effects such as multi-parton interactions, the underlying event and hadronization effects by virtue of their kinematics at lower energies. Some of these effects are negated by the SoftDrop grooming procedure [20]. Jets used in this analysis are minimally biased since no additional selections are applied to the angular threshold. The measurements are fully corrected for detector response via a two-dimensional unfolding procedure. Thus in this letter, for the first time we present fully corrected jet substructure measurements at RHIC that are complementary to the LHC measurements. Additionally, they serve as a crucial baseline for tuning event generators, validating state-of-the-art theoretical calculations of jet functions, and for using similar measurements in heavy-ion collisions to extract medium-modified parton dynamics.

2. Experimental Setup and Jet Reconstruction

The data analyzed in this letter were collected by the STAR experiment [22] in p+p collisions at $\sqrt{s}$ = 200 GeV in 2012. STAR is a cylindrical detector with multiple concentric layers of detector components, including the Time Projection Chamber (TPC) [23] and a Barrel ElectroMagnetic Calorimeter (BEMC) [24], both of which are enclosed in a 0.5 T solenoidal magnetic field. Candidate collision vertices are

reconstructed with charged particle tracks from the TPC. To minimize pileup events and to ensure uniform detector acceptance, only the highest quality primary vertex in each event is selected, and its position along the beam axis is required to fall within $|z_{\mathrm{vertex}}| < 30$ cm from the center of the STAR detector.

Jet finding in this analysis utilizes both the charged particle tracks from the TPC and calorimeter towers from the BEMC. Tracks are required to have more than 52% of possible space points measured in the TPC (up to 45), a minimum of 20 measured space points, a distance of closest approach (DCA) to the primary vertex less than 1 cm, and $|\eta| < 1$. The transverse energies (E_{T}) of electrons, positrons and photons, both directly produced and originating from decays of neutral hadrons, are extracted from the BEMC towers with a granularity of 0.05×0.05 in $\eta - \phi$. The BEMC covers full azimuth within $|\eta| < 1$. Energies deposited by charged particles in the BEMC, including electrons and positrons, are accounted for after a 100% hadronic correction, i.e., the transverse momenta of any charged tracks that extrapolate to a tower are subtracted from the tower E_{T}. Tower energies are set to zero if they become negative via this correction. Events containing tracks with $p_{\mathrm{T}} > 30$ GeV/c were not considered due to the poor momentum resolution for such almost straight (low curvature) tracks in the TPC. For consistency, events with BEMC towers above the same threshold were likewise rejected.

Events were selected online by a BEMC trigger utilizing a patch of calorimeter towers. The BEMC is split into 18 partially overlapping patches, called Jet Patches (JP), covering 1.0×1.0 in $\phi - \eta$. To fulfill the JP requirement, the combined raw ADC counts in at least one of the patches is above a certain threshold corresponding to $\sum E_{\mathrm{T,Tower}} > 7.3$ GeV. With these aforementioned requirements on event selection, we select and analyze about 11 million triggered events.

Towers and charged tracks with $0.2 < E_{\mathrm{T}}(p_{\mathrm{T}}) < 30.0$ GeV(GeV/c) are clustered into jets using the anti-k_{T} algorithm from the FastJet package [25]. Jets are reconstructed with varying resolution parameters, $R = 0.2, 0.4$ and 0.6, and within $|\eta^{\mathrm{jet}}| < 1 - R$ to avoid partially reconstructed jets at the edge of the acceptance. Jets are also required to have no more than 90% of their energies provided by the BEMC towers to ensure good quality. This requirement rejects 3.4% of the reconstructed jets with the effect predominantly occurring at $p_{\mathrm{T,jet}} > 15$ GeV/c. The fully reconstructed

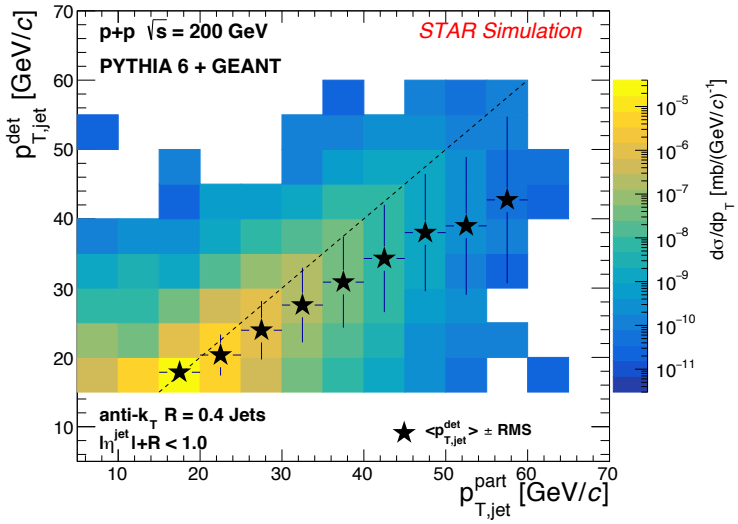

Figure 1: Particle-level jet $p_{\mathrm{T,jet}}^{\mathrm{part}}$ from PYTHIA 6 simulation versus detector-level jet $p_{\mathrm{T,jet}}^{\mathrm{det}}$ from a GEANT simulation of the STAR detector for $R = 0.4$ jets. The data points and the error bars represent the mean $p_{\mathrm{T,jet}}^{\mathrm{det}}$ and the width (RMS) for a given $p_{\mathrm{T,jet}}^{\mathrm{part}}$ selection.

jets that pass the SoftDrop criteria are then considered for the study.

3. Detector Simulation and Unfolding

In order to study the response of the STAR detector to jet substructure observables, p+p events at $\sqrt{s} = 200$ GeV are generated using the PYTHIA 6.4.28 [15] event generator with the Perugia 2012 tune and CTEQ6L PDFs [26]. The PYTHIA 6 used in this analysis was further tuned to match the underlying event characteristics as measured by STAR in a recent publication [27]. These generated events are then passed through a GEANT3 [28] simulation of the STAR detector and embedded into zero-bias data from the same p+p run period. With the GEANT simulated PYTHIA 6 events, identical analysis procedures including event and jet selection criteria mentioned in Sect. 2 are implemented. Jets that are found from PYTHIA 6 simulations before and after the embedding procedures are hereafter referred to as particle-level and detector-level jets, respectively. The long-lived weak-decaying particles, which are not included in the jet finding at the particle level, are simulated in the event generation, and their decay prod-

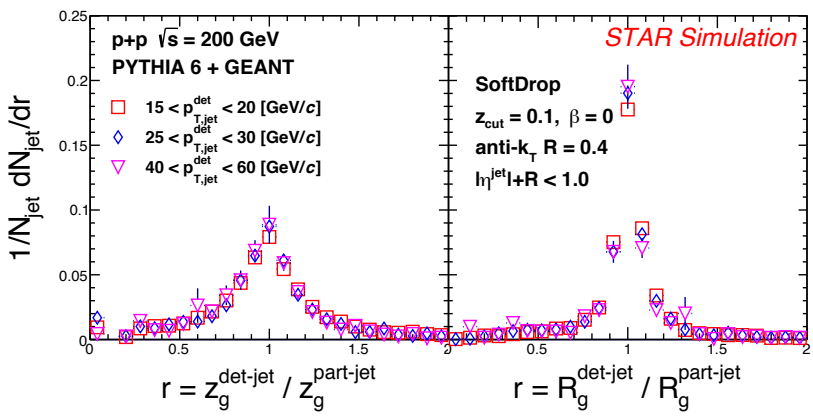

Figure 2: Detector resolutions shown as the ratio of the detector-level to the matched particle-level SoftDrop observables $z_{\rm g}$ (left) and $R_{\rm g}$ (right) for various selections of $p_{\rm T,jet}^{\rm det}$ (varying markers).

ucts are included in the detector-level jets as in real data analysis. The STAR detector response to a jet is estimated by comparing the properties of a PYTHIA 6 particle-level jet with its geometrically matched detector-level jet based on the following matching criterion, $\sqrt{(\Delta\eta)^2 + (\Delta\phi)^2} < R$, where the Δ refers to the difference between the detector- and particle-level jets in the same event and R is the jet resolution parameter. With our jet quality selections, we have about 2% of detector-level jets with $p_{\rm T,jet}^{\rm det} > 15$ GeV/c that cannot be matched to particle-level jets. On the other hand, the jet finding efficiency for particle-level jets varies within 80-94% for $15 < p_{\rm T,jet}^{\rm part} < 60$ GeV/c. The two dimensional $p_{\rm T,jet}$ response matrix for $R = 0.4$ jets is shown in Fig. 1, in which the filled markers represent the average detector-level $p_{\rm T,jet}^{\rm det}$ for a given particle-level $p_{\rm T,jet}^{\rm part}$. In comparison to the dashed diagonal line in Fig. 1, we find the mean $p_{\rm T,jet}^{\rm det}$ to be smaller than the corresponding $p_{\rm T,jet}^{\rm part}$ primarily due to tracking inefficiency. For the jet substructure observables, the detector response is shown in Fig. 2, plotted as the ratio of detector-level jet quantity to the matched particle-level jet quantity for a variety of $p_{\rm T,jet}^{\rm det}$ selections. Cases where one of the jets (matched detector- and particle-level jets) does not pass the SoftDrop criterion are shown in the first bin on the x-axis in the left panel of Fig. 2. The detector resolutions for the SoftDrop observables are peaked at unity, and independent of the $p_{\rm T,jet}^{\rm det}$, which makes it feasible for correcting the measurements

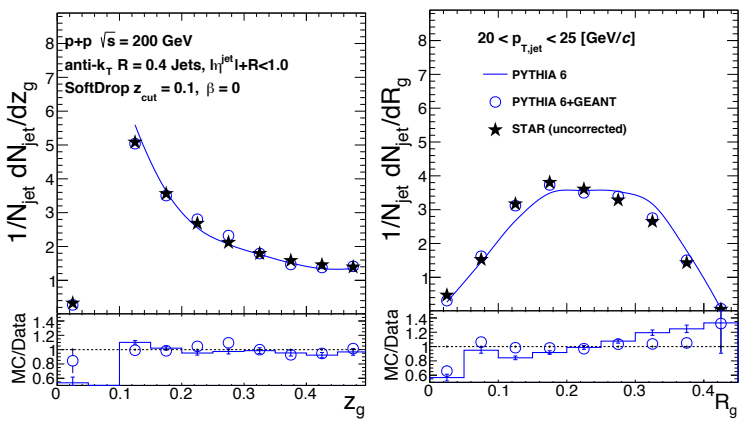

Figure 3: Comparisons of the SoftDrop z_g (left) and R_g (right) distributions in raw data to PYTHIA 6 and PYTHIA 6+GEANT simulations. The bottom panels show the ratio of MC to raw data.

for detector effects via a two-dimensional (e.g., $p_{T,jet}$ and z_g) unfolding procedure.

For anti-k_T, $R = 0.4$ jets with $20 < p_{T,jet} < 25$ GeV/c, the tuned PYTHIA 6 (blue solid line), PYTHIA 6+GEANT simulation (blue open circles) and uncorrected data (filled black star markers) distributions are shown in Fig. 3 for z_g on the left and R_g on the right. The bottom panels show the ratio of simulation to data where we observe a good agreement. In comparing the particle-level and detector-level PYTHIA 6 distributions, we see small but statistically significant differences due to the detector response which we correct for via an unfolding method described below.

The SoftDrop z_g and R_g distributions in this analysis are unfolded to the particle level to correct for detector effects including smearing and bin-by-bin migration. The fact that the detector response peaks at unity and is independent of $p_{T,jet}$, as shown in Fig. 2, generates a more diagonal unfolding matrix in 4 dimensions (i.e., detector- and particle-level $p_{T,jet}$ and z_g or $p_{T,jet}$ and R_g). Two-dimensional Bayesian unfolding [29] is done using the tools available in the RooUnfold package [30] with four iterations to take into account non-diagonal bin-to-bin migrations both in jet p_T and SoftDrop observables. As a consequence of the detector simulation reproducing the uncorrected data as shown in Fig. 3, the unfolding procedure converges and is numerically stable. The priors in the unfolding procedure are taken from the PYTHIA 6 simulation and

their variations are studied as a source of systematic uncertainty.

4. Systematic uncertainties

There are two main categories of systematic uncertainties considered in this analysis. The first is related to the reconstruction performance of the STAR detector, including the uncertainty on the tower gain calibration (3.8%) and the absolute tracking efficiency (4%). The other source of systematic uncertainty is due to the analysis procedure, i.e., the use of hadronic correction (as described in Sec. 2) and the unfolding procedure. The correction to the tower energy, based on the matched tracks' momenta, is varied by subtracting half of the matched tracks' momenta from their corresponding tower E_{T}. With regards to the unfolding procedure, the uncertainties include the variation of the iteration parameter from 2–6 with 4 as the nominal value, and a variation of the input prior shape for z_{g}, R_{g} and p_{T} individually by using PYTHIA 8 and HERWIG 7. We estimated the effect of different sources on the final results by varying the detector simulation, following the same unfolding procedure and comparing to the nominal result. Since we are reporting self-normalized distributions, the luminosity uncertainty with respect to the data-taking is not considered. The total systematic uncertainties for the z_{g} and R_{g} measurements, calculated by adding individual sources in quadrature, are presented in Tab. 1 and 2 for $R = 0.4$ jets in $20 < p_{\mathrm{T,jet}} < 25$ GeV/c range. For both measurements, the largest systematic uncertainty results from the unfolding procedure. The total systematic uncertainties for these softdrop observables decrease slightly as the jet resolution parameter increases.

5. Results

The fully corrected z_{g} and R_{g} measurements are compared to leading order event generators, PYTHIA 6, PYTHIA 8 and HERWIG 7. Since our PYTHIA 6 events do not include weak decays at the particle level, we generate PYTHIA 8 and HERWIG 7 events with the same requirement. We note that for the observables discussed in this letter, we do not observe a significant effect due to weak decays. The parton shower

Source / Range in z_g	Hadronic Correction	Tower Gain	Tracking Efficiency	Unfolding	Total
[0.10, 0.15]	0.4%	2%	1.7%	2.9%	3.9%
[0.25, 0.30]	$\approx$ 0%	2.3%	1.5%	5.2%	5.8%
[0.45, 0.50]	0.6%	1.6%	1.9%	6.8%	7.3%

Table 1: Uncertainties on the SoftDrop z_g measurement for $R = 0.4$ jets with $20 < p_{T,jet} < 25$ GeV/c as a representative jet collection. Each row corresponds to a particular range of z_g.

Source / Range in R_g	Hadronic Correction	Tower Gain	Tracking Efficiency	Unfolding	Total
[0.10 - 0.15]	2%	2.2%	5.6%	7.6%	9.9%
[0.20 - 0.25]	0.5%	1.1%	0.2%	1.9%	2.2%
[0.30 - 0.35]	1.6%	2.8%	2.6%	9.1%	10%
[0.40 - 0.45]	8.4%	2.7%	20.6%	40.3%	46.15%

Table 2: Uncertainties on the SoftDrop R_g measurement. Column and row descriptions are identical to Tab. 1.

implementations are varied amongst the models, with PYTHIA 6 and PYTHIA 8 featuring virtuality ordered shower in contrast to HERWIG 7 with angular ordering. The description of the underlying event in PYTHIA 6 is based on the Perugia 2012 tune [31] and further tuned to match data from RHIC whereas PYTHIA 8 uses the Monash 2013 tune which was based on the LHC data [32]. The HERWIG 7 calculations use the EE4C underlying event tune [33] appropriately scaled for the collision energy at RHIC.

The fully corrected z_{g} measurements for jets of varying $p_{\mathrm{T,jet}}$ are compared to MC predictions as shown in Fig. 4. In addition, we show the symmetrized DGLAP splitting function at leading order for a quark emitting a gluon as the red dashed lines. The different panels represent jets with low $p_{\mathrm{T,jet}}$ in the top middle and high $p_{\mathrm{T,jet}}$ in the bottom right. We observe a more symmetric splitting (larger mean z_{g} or, consequently, a flatter shape) function at lower $p_{\mathrm{T,jet}}$ that gradually tends towards more asymmetric (smaller mean z_{g}) at higher $p_{\mathrm{T,jet}}$. The measurements also indicate a $p_{\mathrm{T,jet}}$-independent z_{g} shape slightly steeper than the theoretical limit around $p_{\mathrm{T,jet}} > 30$ GeV/c within our kinematic range. With symmetric splitting functions, the probability to radiate a high-z gluon (where z is defined as the radiated object's energy fraction with respect to the original parton) is enhanced as opposed to an asymmetric splitting function dominated by low-z emissions. This evolution from a symmetric to asymmetric splitting function with increasing $p_{\mathrm{T,jet}}$ is consistent with pQCD expectation wherein, a high-momentum parton has an enhanced probability to radiate a soft gluon. Such behavior is captured by both angular and virtuality ordered parton shower models. With default hadronization turned on, PYTHIA 6, PYTHIA 8 and HERWIG 7 describe the qualitative shape as observed in these measurements. To compare more quantitatively, the bottom panels show the ratio of the model calculations to data, and the shaded red region represents the total systematic uncertainty in data. Both PYTHIA versions are able to describe the z_{g} measurements. However, HERWIG 7 seems to prefer more symmetric splits, especially at larger $p_{\mathrm{T,jet}}$.

The SoftDrop R_{g} for $R = 0.4$ jets are presented in Fig. 5. The R_{g} shows a momentum-dependent narrowing of the jet structure as reflected in a shift to smaller values as the jet momentum increases. The measured R_{g} distributions are qualitatively reproduced by all event generators. In contrast to the observations from the z_{g} measurement, HER-

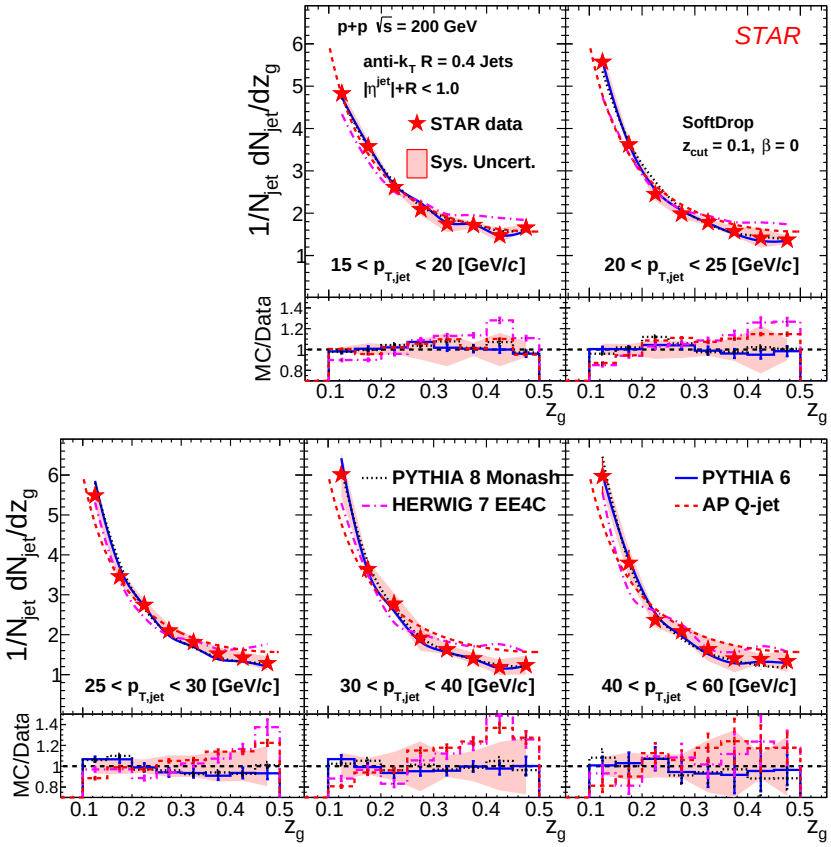

Figure 4: Distribution of the SoftDrop z_g in p+p collisions at $\sqrt{s}$ = 200 GeV for anti-k$_T$ R = 0.4 jets of varying transverse momenta (15 < $p_{T,jet}$ < 20 GeV/c in top middle to 40 < $p_{T,jet}$ < 60 GeV/c in bottom right). The data are in solid red star markers with systematic uncertainties represented as shaded red regions (statistical errors are in most cases smaller than the marker size) and compared to PYTHIA 8 (Monash 2013 Tune, solid black line), PYTHIA 6 (Perugia Tune, solid blue line), and HERWIG 7 (EE4C Tune, solid magenta line). The data are also compared to the DGLAP splitting kernel for quark jets in all the panels shown in red dashed line. The corresponding bottom panels show the ratio of MC to the fully corrected data.

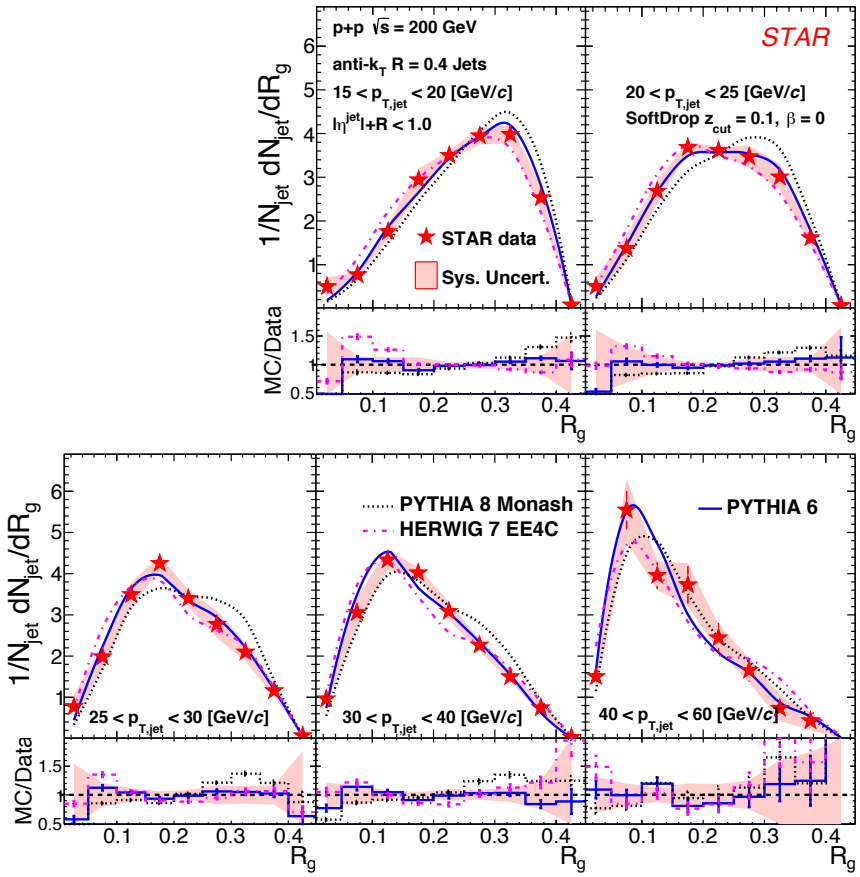

Figure 5: Measurement of the SoftDrop R_g in p+p collisions at $\sqrt{s}$ = 200 GeV for anti-k$_T$ R = 0.4 jets. The various panels and calculations are the same as those described in Fig. 4.

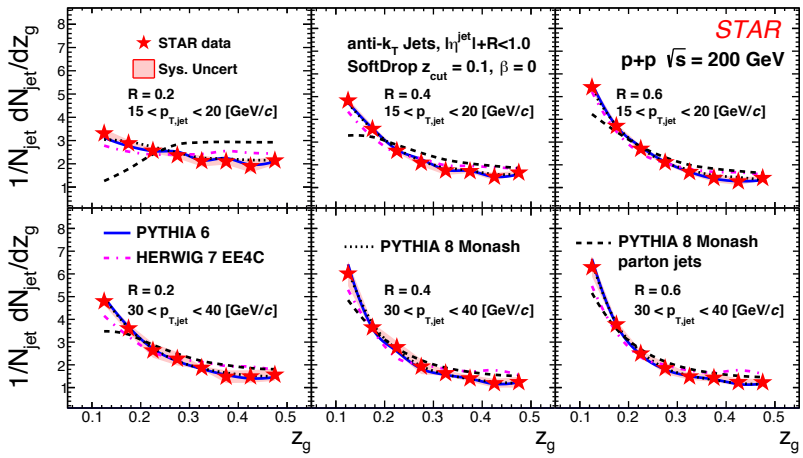

Figure 6: Radial scans of the SoftDrop z_g in p+p collisions at $\sqrt{s}$ = 200 GeV for anti-k$_T$ R = 0.2 (left), R = 0.4 (middle) and R = 0.6 (right) jets of varying transverse momenta ($15 < p_{T,jet} < 20$ GeV/c and $30 < p_{T,jet} < 40$ GeV/c in the top and bottom rows respectively). The data are in solid red star markers with systematic uncertainties represented as shaded red regions (statistical errors are in most cases smaller than the marker size) and are compared to leading order MC generators: PYTHIA 8 (Monash 2013 Tune, solid black line), PYTHIA 6 (Perugia Tune, solid blue line), HERWIG 7 (EE4C Tune, solid magenta line). The data are also compared with PYTHIA 8 parton jets without hadronization in the dashed black line in all the panels.

WIG 7 shows a slight tendency towards smaller R_g, while PYTHIA 8 prefers a systematically wider R_g distribution. For $R = 0.4$ jets, PYTHIA 6 is able to quantitatively describe data, whilst neither PYTHIA 8 nor HERWIG 7 is able to explain both z_g and R_g observables simultaneously within the experimental systematic uncertainties.

We further measured the splitting by varying the jet resolution parameter R as shown in Fig. 6 and Fig. 7 for the z_g and R_g, respectively. The left, middle and right panels represent $R = 0.2, 0.4$ and 0.6 jets. The top row is for jets with $15 < p_{T,jet} < 20$ GeV/c and the bottom row for jets with $30 < p_{T,jet} < 40$ GeV/c. Jets with smaller resolution parameters and at lower $p_{T,jet}$ display stronger z_g shape modification with respect to the ideal DGLAP splitting and do not reproduce the characteristic $1/z$ shape seen at higher $p_{T,jet}$. The narrowing of the R_g with increasing $p_{T,jet}$ becomes more significant for jets of larger resolution parameters. The flattening of the z_g shape for jets with $R = 0.2$ and low $p_{T,jet}$ are due to the stringent kinematic constraints on the phase

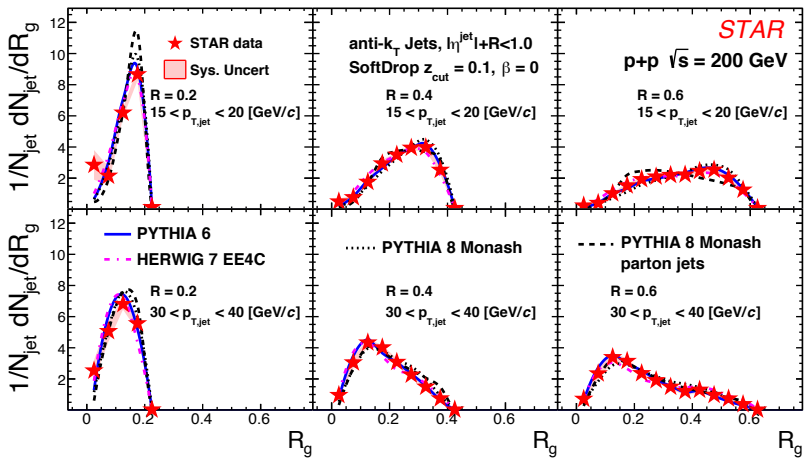

Figure 7: Radial scans of the SoftDrop R_g in p+p collisions at $\sqrt{s}$ = 200 GeV. The different panels and calculations are similar as described in Fig. 6.

space available. This observation is evident by the R_g ranges seen in the top left panel in Fig. 7, for the splitting that is a direct consequence of virtuality/angular ordering. The dashed black curve shows the z_g and R_g distribution from PYTHIA 8 events without hadronization (parton jets). We find that hadronization, as described in PYTHIA 8, tends to create softer z_g or more asymmetric splits. In contrast, we observe the apparent robustness of the R_g observable against hadronization effects.

Due to recent advances in theoretical calculations regarding jets of small resolution parameters and low momenta [34, 35], we can now compare our fully corrected data to predictions at next-to-leading-log accuracy in Fig. 8 for z_g (left panels) and R_g (right panels). The systematic uncertainty in the theoretical calculations (gray shaded band) arises from QCD scale variations, including the p_T-hard scale, the jet scale ($p_{T,jet} \cdot R$) and the scales associated with the substructure observables mentioned here [34]. We note that the systematic uncertainties for the calculations are large for the kinematic range studied in this measurement. These predictions are for jets at the parton level without non-perturbative corrections. This is one possible reason why the comparison to data at low jet momenta and small jet resolution parameter exhibits large deviations in the z_g. On the other hand the predictions for the R_g observable show large discrep-

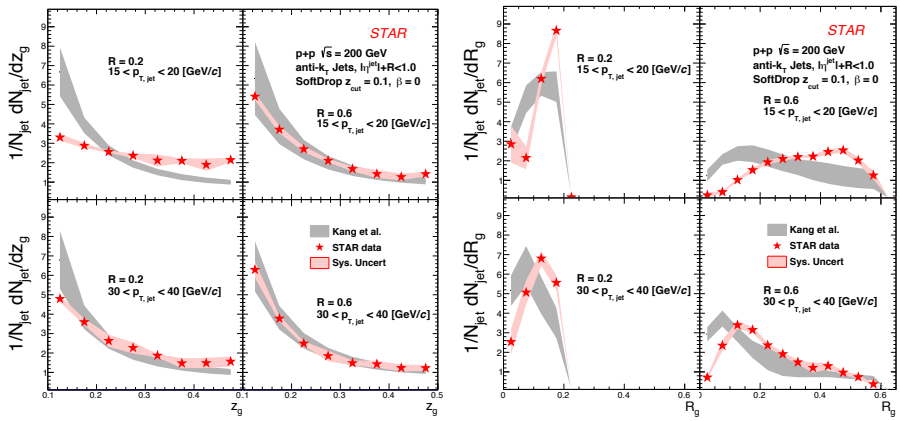

Figure 8: Comparisons of fully corrected STAR data (red markers) for z_{g} (left panels) and R_{g} (right panels) with theoretical calculations at next-to-leading-log accuracy at the parton level shown as gray shaded bands. The top and bottom panels show comparisons for $15 < p_{\mathrm{T,jet}} < 20$ GeV/c and $30 < p_{\mathrm{T,jet}} < 40$ GeV/c respectively. In each of the 4-panel plots, the left and right columns are for jets of $R = 0.2$ and $R = 0.6$.

ancies with the data for all of the jet resolution parameters and kinematics except the largest resolution parameter and highest $p_{\mathrm{T,jet}}$ where the shape gets close to the data. These comparisons highlight the need for more realistic calculations, including corrections arising from non-perturbative effects and higher-order corrections to further understand jet substructure more quantitatively.

6. Summary

In summary, we presented the first fully corrected SoftDrop z_{g} and R_{g} measurements of inclusive jets of varying resolution parameters with $15 < p_{\mathrm{T,jet}} < 60$ GeV/c in p+p collisions at $\sqrt{s} = 200$ GeV. The z_{g} distribution converges towards an approximately $p_{\mathrm{T,jet}}$-independent shape above 30 GeV/c which is slightly more asymmetric than the idealized UV limit. On the other hand, the R_{g} reflects a momentum-dependent narrowing of the jet structure. We observe that lower momentum jets are more likely to have a wider jet structure with more symmetric splitting within the jet. This behavior reverses for higher $p_{\mathrm{T,jet}}$ jets wherein they are narrower and dominated by asymmetric splits. We also note that at small jet resolution parameters and low $p_{\mathrm{T,jet}}$, the z_{g} is sensitive to hadronization effects resulting in a significant enhancement of asymmetric

splitting, whereas for larger resolution parameters, 0.4 and 0.6, the effect is moderate and only results in a minor (shape) change towards more asymmetric splitting. The SoftDrop R_{g} is observed to be less sensitive to hadronization. For both the measurements presented in this letter, we observe that the RHIC-tuned PYTHIA 6 is able to reproduce data whereas PYTHIA 8 and HERWIG 7 are unable to simultaneously describe both scales of the jet evolution. We also showed comparisons to theoretical calculations that extend the predictive power of pQCD at jet scales closer to the fundamental QCD scale, i.e., for jets with small momenta and resolution parameters. Such comparisons to data highlight the need for continued theoretical studies into the exact interplay between measured hadronic jet substructure observables and the underlying partonic splitting at RHIC energies. These studies offer a unique opportunity to further tune MC event generators and for understanding higher order effects on jet evolution at RHIC kinematics.

Acknowledgement

We thank Jesse Thaler, Yacine Mehtar-Tani, Felix Ringer and Zhangbo Kang for useful discussions on the topic of jet substructure and SoftDrop. We thank the RHIC Operations Group and RCF at BNL, the NERSC Center at LBNL, and the Open Science Grid consortium for providing resources and support. This work was supported in part by the Office of Nuclear Physics within the U.S. DOE Office of Science, the U.S. National Science Foundation, the Ministry of Education and Science of the Russian Federation, National Natural Science Foundation of China, Chinese Academy of Science, the Ministry of Science and Technology of China and the Chinese Ministry of Education, the National Research Foundation of Korea, Czech Science Foundation and Ministry of Education, Youth and Sports of the Czech Republic, Hungarian National Research, Development and Innovation Office, New National Excellency Programme of the Hungarian Ministry of Human Capacities, Department of Atomic Energy and Department of Science and Technology of the Government of India, the National Science Centre of Poland, the Ministry of Science, Education and Sports of the Republic of Croatia, RosAtom of Russia and German Bundesministerium fur Bildung, Wis-

senschaft, Forschung and Technologie (BMBF) and the Helmholtz Association.

References

[1] G. Sterman, S. Weinberg, Jets from quantum chromodynamics, Phys. Rev. Lett. 39 (1977) 1436–1439. doi:10.1103/PhysRevLett.39.1436.
URL https://link.aps.org/doi/10.1103/PhysRevLett.39.1436

[2] M. Connors, C. Nattrass, R. Reed, S. Salur, Jet measurements in heavy ion physics, Rev. Mod. Phys. 90 (2018) 025005. arXiv:1705.01974, doi:10.1103/RevModPhys.90.025005.

[3] G.-Y. Qin, X.-N. Wang, Jet quenching in high-energy heavy-ion collisions, Int. J. Mod. Phys. E24 (11) (2015) 1530014, [,309(2016)]. arXiv:1511.00790, doi:10.1142/S0218301315300143,10.1142/9789814663717_0007.

[4] M. Dittmar, et al., Introduction to parton distribution functions.
URL https://cds.cern.ch/record/941455

[5] V. N. Gribov, L. N. Lipatov, Deep inelastic e p scattering in perturbation theory, Sov. J. Nucl. Phys. 15 (1972) 438–450, [Yad. Fiz.15,781(1972)].

[6] Y. L. Dokshitzer, Calculation of the Structure Functions for Deep Inelastic Scattering and e+ e- Annihilation by Perturbation Theory in Quantum Chromodynamics., Sov. Phys. JETP 46 (1977) 641–653, [Zh. Eksp. Teor. Fiz.73,1216(1977)].

[7] G. Altarelli, G. Parisi, Asymptotic Freedom in Parton Language, Nucl. Phys. B126 (1977) 298–318. doi:10.1016/0550-3213(77)90384-4.

[8] M. Dasgupta, A. Fregoso, S. Marzani, G. P. Salam, Towards an understanding of jet substructure, JHEP 09 (2013) 029. arXiv:1307.0007, doi:10.1007/JHEP09(2013)029.

[9] A. J. Larkoski, S. Marzani, G. Soyez, J. Thaler, Soft Drop, JHEP 05 (2014) 146. arXiv:1402.2657, doi:10.1007/JHEP05(2014)146.

[10] A. J. Larkoski, S. Marzani, J. Thaler, Sudakov Safety in Perturbative QCD, Phys. Rev. D91 (11) (2015) 111501. arXiv:1502.01719, doi:10.1103/PhysRevD.91.111501.

[11] Y. L. Dokshitzer, G. D. Leder, S. Moretti, B. R. Webber, Better jet clustering algorithms, JHEP 08 (1997) 001. arXiv:hep-ph/9707323, doi:10.1088/1126-6708/1997/08/001.

[12] M. Wobisch, T. Wengler, Hadronization corrections to jet cross-sections in deep inelastic scattering, in: Monte Carlo generators for HERA physics. Proceedings, Workshop, Hamburg, Germany, 1998-1999, 1998, pp. 270–279. arXiv:hep-ph/9907280.

[13] A. Larkoski, S. Marzani, J. Thaler, A. Tripathee, W. Xue, Exposing the QCD Splitting Function with CMS Open Data, Phys. Rev. Lett. 119 (13) (2017) 132003. arXiv:1704.05066, doi:10.1103/PhysRevLett.119.132003.

[14] A. M. Sirunyan, et al., Measurement of the Splitting Function in pp and Pb-Pb Collisions at $\sqrt{s_{\rm NN}}$ = 5.02 TeV, Phys. Rev. Lett. 120 (14) (2018) 142302. arXiv:1708.09429, doi:10.1103/PhysRevLett.120.142302.

[15] T. Sjostrand, S. Mrenna, P. Z. Skands, PYTHIA 6.4 Physics and Manual, JHEP 05 (2006) 026. arXiv:hep-ph/0603175, doi:10.1088/1126-6708/2006/05/026.

[16] T. Sjstrand, S. Ask, J. R. Christiansen, R. Corke, N. Desai, P. Ilten, S. Mrenna, S. Prestel, C. O. Rasmussen, P. Z. Skands, An Introduction to PYTHIA 8.2, Comput. Phys. Commun. 191 (2015) 159–177. arXiv:1410.3012, doi:10.1016/j.cpc.2015.01.024.

[17] M. Bahr, et al., Herwig++ Physics and Manual, Eur. Phys. J. C58 (2008) 639–707. arXiv:0803.0883, doi:10.1140/epjc/s10052-008-0798-9.

[18] J. Bellm, et al., Herwig 7.0/Herwig++ 3.0 release note, Eur. Phys. J. C76 (4) (2016) 196. arXiv:1512.01178, doi:10.1140/epjc/s10052-016-4018-8.

[19] G. Milhano, U. A. Wiedemann, K. C. Zapp, Sensitivity of jet substructure to jet-induced medium response, Phys. Lett. B779 (2018) 409–413. arXiv:1707.04142, doi:10.1016/j.physletb.2018.01.029.

[20] C. Frye, A. J. Larkoski, M. D. Schwartz, K. Yan, Factorization for groomed jet substructure beyond the next-to-leading logarithm, JHEP 07 (2016) 064. arXiv:1603.09338, doi:10.1007/JHEP07(2016)064.

[21] X. Liu, S.-O. Moch, F. Ringer, Phenomenology of single-inclusive jet production with jet radius and threshold resummation, Phys. Rev. D97 (5) (2018) 056026. arXiv:1801.07284, doi:10.1103/PhysRevD.97.056026.

[22] K. Ackermann, et al., STAR Detector overview, Nucl. Instrum. Meth. A499 (2003) 624–632. doi:10.1016/S0168-9002(02)01960-5.

[23] M. Anderson, et al., The Star time projection chamber: A Unique tool for studying high multiplicity events at RHIC, Nucl. Instrum. Meth. A499 (2003) 659–678. arXiv:nucl-ex/0301015, doi:10.1016/S0168-9002(02)01964-2.

[24] M. Beddo, et al., The STAR barrel electromagnetic calorimeter, Nucl. Instrum. Meth. A499 (2003) 725–739. doi:10.1016/S0168-9002(02)01970-8.

[25] M. Cacciari, G. P. Salam, G. Soyez, The Anti-k(t) jet clustering algorithm, JHEP 04 (2008) 063. arXiv:0802.1189, doi:10.1088/1126-6708/2008/04/063.

[26] H. L. Lai, J. Huston, S. Kuhlmann, J. Morfin, F. I. Olness, J. F. Owens, J. Pumplin, W. K. Tung, Global QCD analysis of parton structure of the nucleon: CTEQ5 parton distributions, Eur. Phys. J. C12 (2000) 375–392. arXiv:hep-ph/9903282, doi:10.1007/s100529900196.

[27] J. Adam, et al., Longitudinal double-spin asymmetry for inclusive jet and dijet production in pp collisions at $\sqrt{s} = 510$ GeV, Phys. Rev. D100 (5) (2019) 052005. arXiv:1906.02740, doi:10.1103/PhysRevD.100.052005.

[28] R. Brun, F. Bruyant, F. Carminati, S. Giani, M. Maire, A. McPherson, G. Patrick, L. Urban, GEANT Detector Description and Simulation Tool. doi:10.17181/CERN.MUHF.DMJ1.

[29] G. D'Agostini, A Multidimensional unfolding method based on Bayes' theorem, Nucl. Instrum. Meth. A362 (1995) 487–498. doi:10.1016/0168-9002(95)00274-X.

[30] RooUnfold root unfolding framework, http://hepunx.rl.ac.uk/~adye/software/unfold/RooUnfold.html#refs, accessed: 2019-03-06.

[31] P. Z. Skands, Tuning Monte Carlo generators: The Perugia tunes, Phys. Rev. D 82 (2010) 074018. arXiv:1005.3457v5, doi:10.1103/PhysRevD.82.074018. URL https://link.aps.org/doi/10.1103/PhysRevD.82.074018

[32] P. Skands, S. Carrazza, J. Rojo, Tuning PYTHIA 8.1: the Monash 2013 Tune, Eur. Phys. J. C74 (8) (2014) 3024. arXiv:1404.5630, doi:10.1140/epjc/s10052-014-3024-y.

[33] M. H. Seymour, A. Siodmok, Constraining MPI models using σ_{eff} and recent Tevatron and LHC Underlying Event data, JHEP 10 (2013) 113. arXiv:1307.5015, doi:10.1007/JHEP10(2013)113.

[34] Z.-B. Kang, K. Lee, X. Liu, D. Neill, F. Ringer, The soft drop groomed jet radius at NLL.arXiv:1908.01783.

[35] A. Tripathee, W. Xue, A. Larkoski, S. Marzani, J. Thaler, Jet Substructure Studies with CMS Open Data, Phys. Rev. D96 (7) (2017) 074003. arXiv:1704.05842, doi:10.1103/PhysRevD.96.074003.